A bioengineering approach to Schlemm's canal-like stem cell differentiation for *in vitro* glaucoma drug screening

Yangzi Isabel Tian[a], **Xulang Zhang**[a], **Karen Torrejon**[b], **John Danias**[c], **Sofya Gindina**[c], **Ashima Nayyar**[c], **Yiqin Du**[d], **Yubing Xie**[a,1]

[a]Colleges of Nanoscale Science and Engineering, SUNY Polytechnic Institute, 257 Fuller Road, Albany, NY 12203, USA

[b]Glauconix Biosciences, Inc., 251 Fuller Road, Albany, NY 12203, USA

[c]SUNY Downstate Medical Center, 450 Clarkson Ave, Brooklyn, NY 11203, USA

[d]University of Pittsburg School of Medicine, 203 Lothrop Street, Pittsburgh, PA 15213, USA

Abstract

Human Schlemm's canal (HSC) cells are critical for understanding outflow physiology and glaucoma etiology. However, primary donor cells frequently used in research are difficult to isolate. HSC cells exhibit both vascular and lymphatic markers. Human adipose-derived stem cells (ADSCs) represent a potential source of HSC due to their capacity to differentiate into both vascular and lymphatic endothelial cells, via VEGF-A and VEGF-C. Shear stress plays a critical role in maintaining HSC integrity, function, and PROX1 expression. Additionally, the human trabecular meshwork (HTM) microenvironment could provide cues for HSC-like differentiation. We hypothesize that subjecting ADSCs to VEGF-A or C, shear stress, and co-culture with HTM cells could provide biological, mechanical, and cellular cues necessary for HSC-like differentiation. To test this hypothesis, effects of VEGF-A, VEGF-C, and shear stress on ADSC differentiation were examined and compared to primary HSC cells in terms of cell morphology, and HSC marker expression using qPCR, immunoblotting, and immunocytochemistry analysis. Furthermore, the effect of co-culture with HTM cells on porous scaffolds on ADSC differentiation was studied. Treatment with VEGF-C under shear stress is effective in differentiating ADSCs into PROX1-expressing HSC-like cells. Co-culture with HTM cells on porous scaffolds leads to HTM/

---

[1]Corresponding author Yubing Xie, Ph.D., Associate Professor, Colleges of Nanoscale Science and Engineering, SUNY Polytechnic Institute, 257 Fuller Road, Albany, NY 12203, USA, Phone: (518) 956-7381, Fax: (518) 956-8687, YXie@sunypoly.edu.

Disclosure: K.T., J.D. and Y.X.: patent: Bioengineered human trabecular meshwork for biological applications, US9506907B2; patent application: Use of vascular cells to create the conventional outflow tract, WO2017130178A3.
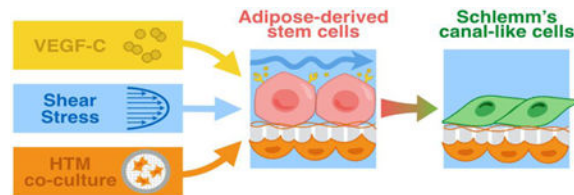
Declaration of interests

The authors declare the following financial interests/personal relationships which may be considered as potential competing interests:

ADSC-derived HSC-like constructs that regulate through-flow and respond as expected to dexamethasone.

Graphical Abstract

Keywords

microfabrication; shear stress; stem cell; Schlemm's canal; glaucoma

1. Introduction

Primary open angle glaucoma is a complex neurodegenerative disease often associated with elevated intraocular pressure (IOP) [1]. As the leading cause of blindness and visual impairment, it affects more than 70 million individuals worldwide [2]. However, while most of the currently available glaucoma therapies target aqueous humor production or the uvealscleral outflow pathway, they do not address the primary conventional outflow pathway, which is normally responsible for 70–90% of aqueous humor drainage into the systemic circulation [3, 4]. Dysfunction and blockage in this primary pathway can lead to increased outflow resistance, elevated IOP, and eventually glaucoma. Although pathogenetic mechanisms that lead to IOP elevation are still unclear, previous studies have identified the inner wall region of Schlemm's canal in conjunction with juxtacanalicular tissue (JCT) region of the trabecular meshwork as the primary site of outflow resistance [5–8].

The inner wall region of Schlemm's canal is composed of the inner wall endothelium of Schlemm's canal, its discontinuous basement membrane, and the adjacent juxtacanalicular connective tissue of the trabecular meshwork [8]. Schlemm's canal is a ring-shaped, often non-continuous vessel that encircles the ocular anterior chamber at the iridocorneal angle. Its lumen is lined with a single non-fenestrated layer of endothelial cells, with their long axis aligned and parallel to the direction of flow [9]. As the final barrier to aqueous humor drainage, the inner wall Schlemm's canal cells experience a remarkably dynamic microenvironment, due to both the shear flow and basal-to-apical flow of aqueous humor through the Schlemm's canal endothelial cells [10–12]. The basal-to-apical flow for the Schlemm's canal cells, in particular, generates a massive transcellular mechanical load, leading to the creation of fluid-filled intracellular cavities or "giant vacuoles" that fuse with the cell membrane [13, 14]. These pressure-dependent protrusions into the canal lumen are often accompanied by transcellular and/or paracellular pores, which allow aqueous humor drainage without compromising the blood-aqueous barrier [15]. In glaucomatous eyes, changes in Schlemm's canal cell contractility and basement membrane stiffness significantly impede giant vacuole and pore formation and lead to increased outflow resistance and IOP elevation [16]. Understanding the underlying mechanism and role of Schlemm's canal cells

in IOP modulation could lead to the development of effective targets for new pharmacologic agents [17].

Isolated primary human Schlemm's canal (HSC) cells provide a valuable *in vitro* cellular model to study their role in outflow physiology and pathology and in discovering new therapeutic targets [18]. In fact, HSC isolated from healthy and glaucomatous eyes have measurable differences in gene expression and cytoskeletal stiffness that affect pore density and outflow resistance [19]. New IOP-lowering agents that include actin depolymerizers and Rho kinase inhibitors target and regulate cell stiffness affecting HSC cells [20, 21]. Unfortunately, HSC cell scarcity and technical difficulty in their isolation creates a bottleneck for effective and affordable high-throughput drug screening using HSC cells. Stem cell differentiation is a promising approach to create an alternative source that is physiologically and functionally similar to HSC cells for *in vitro* cell-based drug screening.

Adipose tissue-derived stem cells (ADSCs) are adult stem cells with the ability to proliferate, self-renew and differentiate [22]. They can be easily isolated from adipose tissue, which can be obtained in large quantity through liposuction, a commonly performed, low-risk surgical procedure [23]. To date, ADSCs have been successfully differentiated into adipocytes [24, 25], osteoblasts [26, 27], chondrocytes [28, 29], myocytes [30, 31], smooth muscle cells [32], neurons [33, 34], vascular endothelium [35–37] and lymphatic endothelium-like cells [38, 39] under lineage-specific culture conditions. In particular, the capacity of ADSCs to differentiate into vascular and lymphatic endothelium-like cells makes them a promising candidate for HSC-like cell differentiation since HSC cells exhibit a combination of vascular and lymphatic phenotypes. Schlemm's canal barrier integrity and functions depend on the induction and continual expression of PROX1, a master regulator of the lymphatic system, and VEGFR3, the surface receptor for vascular endothelial growth factors (VEGFs) [40–42]. Short term treatment using VEGF-C has been shown to induce expression of both vascular endothelial markers (CD31) and lymphatic markers (PROX1) in ADSCs, but not VEGFR-3 [43]. Fluid shear stress on the other hand is known to activate VEGFR-3 expression in both blood and lymphatic endothelial cells [44]. In addition to growth factor and fluid flow, cellular substrate stiffness, composition, and porosity could also alter the three-dimensional microenvironment needed for differentiation [45, 46]. Previously, we have shown that HTM cultured on microporous SU8 scaffolds maintained its *in vivo* phenotype, along with the ability to secrete extracellular matrix (ECM), regulate outflow facility and respond to IOP-altering agents [47–50], making it the ideal cellular substrate to support and guide ADSC differentiation into Schlemm's canal-like cells.

In this study, we tested the hypothesis that ADSCs can be differentiated into HSC-like cells that not only express both vascular and lymphatic markers, but also maintain comparable outflow resistance. VEGF-A (for vascular endothelial differentiation), VEGF-C (for lymphatic endothelial differentiation), shear stress, and co-culture with primary HTM cells were used to promote HSC-like differentiation by mimicking the biological, mechanical and cellular microenvironment *in vivo.* Schlemm's canal cell-like phenotypes were subsequently evaluated by examining the cell morphology using optical and scanning electron microscopy (SEM), gene/protein expression of the HSC marker (e.g., PROX1) using

immunocytochemistry, immunoblotting and qPCR analysis, and functional assessment of outflow facility using perfusion studies.

2.   Materials and methods

2.1   Collection, Isolation, and Culture of Human ADSCs

Human ADSCs were isolated and cultured as described previously [51]. Briefly, human subcutaneous adipose tissue was obtained from patients undergoing elective lipoaspiration surgery with informed consent under a protocol approved by the Institutional Review Board (IRB) of the University of Pittsburgh, consistent with the principles of the Declaration of Helsinki. ADSCs were initially expanded in 75 cm^2 cell culture flasks and fed every 48 hours with 10% FBS (HyClone; Fisher Scientific, Pittsburg, PA) in DMEM/F21 (Gibco, Grand Island, NY) with 100 nM dexamethasone. Cells were maintained at 37°C in a humidified atmosphere with 5% CO_2 until 80–90% confluence, and subcultured using 0.05% trypsin/0.5 mM EDTA (Gibco, Grand Island, NY).

2.2   Primary Human Schlemm's Canal Cell Culture

Primary HSC cells were provided by Dr. Stamer at Duke University. The protocol for HSC cell extraction from post mortem human eyes is described in detail elsewhere [18]. Extracted cells were shipped overnight in T-25 flasks filled with DMEM/Low glucose (Life Technologies; Carlsbad, CA) medium with 10% FBS (Atlas Biologicals, Fort Collins, CO) and 1% penicillin/streptomycin. Upon arrival, the culture medium was replaced with fresh medium and flasks were stored in the incubator at 37°C and 5% CO_2. Medium were changed every other day. Cells were trypsinized and passaged at 1:3 ratio when 80% confluent. All studies were conducted using cells before the 6th passage.

2.3   Primary Human Trabecular Meshwork Cell Culture

Primary HTM cells were isolated from donor tissue rings discarded after penetrating keratoplasty. Isolation of these cells was performed under an IRB-exempt protocol approved by the SUNY Downstate IRB. Isolation and culture conditions were as previously described [47]. All HTM cell strains were characterized as recommended by a consensus of investigators in the field [52], e.g., expression of αB-crystallin and α-smooth muscle actin (αSMA), myocilin induction in response to dexamethasone (Fig.S1). HTM cells were initially expanded in 75 cm^2 cell culture flasks coated with 1% gelatin and fed every 48 hours with 10% FBS (Atlas Biologicals, Fort Collins, CO) in Improved MEM (Corning Cellgro, Manassas, VA) with 1% gentamicin. All studies were conducted using cells before the 5th passage.

2.4   Differentiation of Human ADSCs

The protocol for endothelial differentiation of human ADSCs was modified from a previous study [53]. Briefly, human ADSCs were passaged onto 6-well plates and cultured for 3 days under static conditions in the ADSC medium described above. When culture was 50% confluent, the ADSC medium was exchanged with EGM-2MV (Endothelial Cell Growth Medium BulletKit™; Lonza, Walkersville, MD) supplemented with 50 ng/ml of VEGF-A (Sigma-Aldrich, St Louis, MO). Then the plate was secured onto an orbital shaker (Scilogex,

Rocky Hill, CT) and maintained at 37°C, 5% CO_2. Plates were rotated at 210 cycles/min producing roughly 12 dynes at the periphery of the wells, representing the average shear noted within the human common femoral artery [53, 54], which is comparable to the level of shear flow in Schlemm's canal. Shear stress was applied for 11 days, and the medium was changed every 2 days. Experiments were performed in triplicate and repeated three times.

The protocol for Schlemm's canal-like differentiation also began with passaging human ADSCs onto a 6-well plate with a glass coverslip and culturing for 3 days under static conditions. When culture reached 50% confluence, the ADSC medium was supplemented with 50 ng/ml VEGF-C (Sigma-Aldrich) and subjected to the same amount of shear stress for 11 days. All other cell culture parameters were kept the same as endothelial differentiation. Vehicle-treated ADSCs were used as the control. Experiments were performed in triplicate and repeated three times.

2.5 Microfabrication of SU8 Scaffolds

The microporous, free-standing SU8 scaffolds used for cell culture were microfabricated as described previously [47]. Briefly, a release layer was first spin-coated onto the silicon wafer and baked between 120–150°C. Next, SU8 2010 negative-tone photoresist (MicroChem Corp., Newton, MA) was spin-coated onto the release layer to a thickness <5 μm, baked at 95°C, then cooled to room temperature. The photoresist was exposed to UV-light (140 mJ/cm^2) through a custom-designed mask with the desired pattern, baked at 95°C, and developed in PGMEA (MicroChem Corp.) Finally, the scaffolds were removed from the release layer, rinsed with isopropyl alcohol, and air dried.

2.6 Co-culture with HTM cells on SU8 Scaffolds

Prior to use in cell culture, SU8 scaffolds were mounted on aluminum tape rings, UV sterilized, coated with 1% gelatin to promote cell attachment. Primary HTM cells were seeded at a density of 50,000 cells/scaffold and cultured in HTM medium for 7 days. For co-culture, the scaffold was flipped upside-down, seeded with either human ADSC or HSC cells, and cultured for an additional 7–11 days in HTM medium or until confluency. Primary HTM cells seeded on one side of the scaffold were used as control.

2.7 Optical and Scanning Electron Microcopy

Cell growth was monitored on a daily basis using a Nikon TS100-F inverted microscope (Micro Video Instrument, Avon, MA). Cell morphology was characterized via a LEO 1550 field emission scanning electron microscope (SEM; Leo Electron Microscopy Ltd, Cambridge, UK). To prepare for SEM, samples were fixed with 2% glutaraldehyde solution in 0.1 M phosphate buffer and 0.1 M sucrose for 2 hours at room temperature. Then, samples were chemically dehydrated in a graded ethanol and slowly infiltrated with a graded hexamethyldisilazane (HMDS)-ethanol. Critically dried samples were mounted on SEM stubs using carbon tape and were sputter-coated with iridium to eliminate charging effects. Images were collected at 3 kV gun voltage and working distance of 5 mm. Cell alignment was quantified using the ImageJ plugin, OrientationJ Analysis and Distribution, which creates histogram of cell orientation based on the SEM images. The standard deviation of

the histogram was calculated to represent the alignment index, where high alignment index indicates random orientation and low alignment index indicates similar orientation.

2.8 Immunocytochemistry Analysis

Samples were fixed in 4% paraformaldehyde, permeabilized with 0.2% Triton X-100, and blocked using 5% bovine serum. Samples were subsequently incubated with the appropriate primary antibodies: rabbit anti-CD31, goat anti-VEGFR2, rabbit anti-PROX1, mouse anti-Vimentin, rabbit anti-myocilin, mouse anti-αSMA, rabbit anti-OCT3/4 (Abcam, Cambridge, MA). Secondary antibodies: mouse anti-rabbit Alexa Fluor 488 was used to detect CD31, mouse anti-goat Alexa Fluor 647 was used to detect VEGFR2, mouse anti-rabbit Alexa Fluor 647 was used to detect PROX1, myocilin and OCT3/4, and goat anti-mouse Alexa Fluor 594 was used to detect vimentin and aSMA (1:200, Invitrogen, Grand Island, NY). These samples were further counter-stained with 4,6-diamidino-2-phenylindole (DAPI) to reveal cell nuclei. Laser scanning confocal microscopy was performed using a Leica SP5 confocal microscope, and images were acquired at 20x or 63X magnifications using an oil-immersion objective. Confocal images were processed using Leica LasAF software, and all confocal images within a given experiment were imaged and captured using the same laser intensity and gain settings in order to be able to compare intensities across samples.

2.9 Quantitative real-time PCR Analysis

Total RNA was extracted using RNeasy Mini Kit as per the manufacturer's instructions (Qiagen, Hilden, Germany). RNA was quantified using a NanoDrop ND1000 Spectrophotometer (Thermo Scientific, Wilmington, DE). PCR probes and primers were generated using Integrated DNA Technologies probe/primer design software (http://www.idtdna.com/pages/products/geneexpression/primetime-qpcr-assays-and-primers). Specific primer sequences are listed in Table 1. qRT-PCR was carried out as directed using StepOnePlusTM Real Time PCR system (Applied Biosystems, Foster City, CA). Samples were amplified using a SYBR® green I PCR master mix. Reactions were analyzed in triplicate and expression levels were normalized to the housekeeping gene GAPDH. Relative quantitative data analysis was performed using the comparative Ct, with GAPDH as the endogenous reference. Experiments were run in triplicate and the average values are presented as mean ± standard error of the mean.

2.10 Protein Extraction and Western Blot Analysis

Cellular proteins were extracted with ice-cold radioimmunoprecipitation assay (RIPA) buffer containing protease inhibitors (Complete Protease Inhibitor; Roche, Manheim, Germany). Proteins were quantified by bicinchoninic acid assay (Thermo Fischer Scientific). 20 μg of proteins from each sample were separated by SDS polyacrylamide gel electrophoresis on a 12% gel in MOPS running buffer (ThermoFisher Scientific), transferred onto a nitrocellulose membrane, and probed with primary antibodies against PROX1, CD31, OCT3/4, and β-actin (Abcam). After incubation in HRP-conjugated goat anti-mouse or anti-rabbit secondary antibodies (Invitrogen), bound antibodies were detected using FluorChem E (Protein Simple). Protein expression was analyzed by densitometry using ImageJ, and normalized to the house-keeping β-actin.

2.11 Perfusion Studies

A perfusion apparatus was used as previously described [47]. Samples were securely placed in the perfusion chamber and perfused at various rates for 5 hrs per flow rate (2, 4, 8, and 16 mL/min). Samples, including HTM cells alone, HTM/ADSC-derived HSC-like constructs, and HTM/HSC constructs, were perfused in an apical-to-basal direction for HTM (i.e. basal-to apical direction for HSC-like cells) with perfusion medium consisting of DMEM (Cellgro) with 0.1% gentamicin in the absence or presence of 100 nM dexamethasone which is known to increase outflow resistance/decrease outflow facility and used for trabecular meshwork cell characterization and validation. Pressure was continuously monitored and recorded. After perfusion, samples were fixed and stained for SEM or confocal imaging. The "outflow facility" of the bioengineered HTM and co-culture models was calculated from the inverse of the slope of the pressure versus flow graph, per unit surface area. Six sample replicates per condition were studied under perfusion.

2.12 Statistical Analysis

All experimental data, unless otherwise specified, were expressed as means $\pm$ SEM from at least three independent experiments. Multiple comparisons were performed using two-way ANOVA. p-values of <0.05 were taken to indicate statistical significance.

3. Results

3.1 Initial Endothelial Differentiation of Human ADSCs

To demonstrate their differentiation potential toward endothelial-like cells, human ADSCs were seeded and grown in ADSC medium for three days, then cultured in EGM-2V medium supplemented with VEGF-A in the presence or absence of shear stress for 11 more days. After 3-day treatment, cells started to show morphological changes (Fig. 1A, C, E, G). After 11-day treatment, significant morphological changes were observed in the treated ADSCs (Fig. 1D, F, H) versus the vehicle-treated ADSC control (Fig. 1B). While the morphology in all treated samples became more elongated and directional, ADSCs exposed to both VEGF-A and shear stress formed robust cord-like structures throughout the culture (Fig. 1H). ADSCs that underwent shear stress alone also formed some cords after 11-day treatment (Fig. 1F), but not as robustly when compared to the combined treatment.

These changes in cell morphology were echoed in gene and protein expression analysis as shown in Fig. 2. ADSCs exposed to 11-day treatment with VEGF-A and shear stress significantly increased expression of endothelial markers CD31 and VEGFR2 at both protein (compared Fig. 2D with Fig. 2A–C) and gene level (Fig. 2E and F; CD31: 5-fold; VEGFR2: 17-fold). The gene expression of OCT3/4 in ADSCs treated with shear stress alone or combined with VEGF-A decreased compared to vehicle-treated control although the OCT3/4 gene expression level was not significant compared to the control (Fig. 2G). Interestingly, CD31 and VEGFR2 were minimally expressed in ADSCs treated with VEGF-A alone, as detected by both qPCR and immunocytochemistry analysis (Fig. 2B, E and F). The decreased level of pluripotency marker OCT3/4 gene expression as shown in Fig. 2G indicates that ADSCs treated with VEGF-A underwent differentiation but probably not endothelial differentiation due to the lack of CD31 and VEGFR2 expression.

3.2 Differentiation of ADSCs towards Schlemm's canal-like cells

Given the multipotent nature of human ADSCs, we further investigated their ability to become Schlemm's canal-like cells by inducing lymphatic endothelial differentiation using VEGF-C in the presence or absence of shear stress. VEGF-C was previously successfully used in differentiating ADSCs into lymphatic-like endothelial cells [43, 55]. As shown in Fig. 3, the morphologic transition of ADSCs from a fibroblast-like appearance (Fig. 3A and B) to a typical endothelial cell-specific appearance seen in HSC cells (Fig. 3I and J) could be clearly observed in ADSCs exposed to 11-day treatment with VEGF-C (Fig. 3C and D), shear stress (Fig. 3E and F) or both (Fig. 3G–H). ImageJ was used to quantify the degree of cell orientation using alignment index. While vehicle-treated ADSCs were randomly organized, ADSCs exposed to both VEGF-C and shear stress showed low level alignment index, indicating directionality and higher degree of cell alignment/orientation, comparable to that of primary HSCs (Fig. 3K).

HSC exhibits a combination of blood, vascular, and lymphatic markers [42]. To verify HSC-like differentiation of human ADSCs, we evaluated the gene expression using qPCR analysis of both lymphatic markers (PROX1 and VEGFR3) and vascular markers (CD31 and VEGFR2), along with stem cell marker Oct3/4 after 11-day treatment with VEGF-C and shear stress. As shown in Fig. 4A–D, in comparison to vehicle-treated ADSCs, the mRNA expression level of PROX1, VEGFR3, CD31 and VEGFR2 was increased by 4.61-fold, 1.23-fold, 0.80-fold, and 0.03-fold in VEGF-C treated ADSCs, respectively; 3.11-fold, 1.75-fold, 2.06-fold, and 3.57-fold for ADSCs under shear stress, respectively; and 7.11-fold, 3.99-fold, 2.94-fold, and 4.06-fold for ADSCs exposed to both shear stress and VEGF-C treatment.

Western blot analysis revealed a noticeable increase in the level of PROX1 after 11-day co-treatment with VEGF-C and shear stress (Fig. 4E and F). Expression of OCT3/4, a stem cell pluripotency marker, decreased in the treated groups when compared to the vehicle-treated ADSC control, confirming that these induced ADSCs are undergoing differentiation (Fig. 4G). These protein level expression changes were also captured in immunocytochemistry analysis after 11-day treatment with VEGF-C, shear stress, or both (Fig. 5). Among these conditions, ADSCs co-treated with VEGF-C and shear stress exhibited a similar protein expression profile to primary HSC cells, including aligned cytoskeleton F- actin organization, increased lymphatic marker PROX1 (compare Fig. 5D to 5E), decreased stem cell marker OCT3/4 (compare Fig. 5I to 5J), and comparable expression pattern of vascular marker CD31 and trabecular meshwork marker αSMA (compare Fig. 5N and 5O). These results confirmed that the synergistic treatment with VEGF-C and shear stress can induce ADSC differentiation into HSC-like cells.

3.3 Co-culture with HTM on SU8 scaffolds for Schlemm's canal-like cells differentiation

In addition to biological and mechanical cues such as VEGF-C and fluidic shear stress, we also investigated the role of cellular microenvironment in directing HSC-like differentiation of ADSCs. *In vivo,* HSC endothelial cells form a layer underneath the trabecular meshwork tissue, exchanging signaling through the basement membrane and regulating aqueous humor outflow together. As described previously, the trabecular microenvironment was mimicked

by culturing primary HTM cells on microfabricated, well-defined, porous SU8 to recreate HTM-scaffold constructs. The HTM grown on the SU8 scaffold could support primary HSC cells to grow into a continuous cell layer on the other side of the SU8 scaffold to form a HTM/HSC construct [56]. Similarly, the 3D HTM also allowed ADSCs to grow and differentiate on the other side of the SU8 scaffold to form a HTM/ADSC-derived HSC-like construct. Since our preliminary study showed there was no significant difference in the outflow facility of HTM cells grown on one side or both sides of the scaffold (Fig. S2), we chose HTM cells grown on one side of the SU-8 scaffold as the control.

To evaluate whether these ADSC-derived HSC-like cells could regulate outflow, a perfusion study was performed using a porous SU8 scaffold as the cell culture substrate. Perfusion results for HTM alone and co-culture with HSC cells and ADSC-derived HSC-like cells decreased outflow facility significantly for the co-culture when compared to HTM alone, indicating that the addition of HSC or ADSC-derived cell layer to the HTM outflow model could simulate the flow resistance from the HSC endothelial lining *in vivo.* Interestingly, the outflow facilities of both ADSC-derived HSC-like cells and primary HSC cells were very similar (Fig. 6), suggesting ADSCs co-cultured with HTM cells on scaffolds could be a potential alternative to the HTM/HSC construct for mimicking the ocular outflow tract.

Immunocytochemistry analysis was further performed to examine HTM and HSC markers in these HTM, HTM/HSC and HTM/ADSC-derived HSC-like constructs (Fig. 7A–F). HTM alone expressed HTM markers of myocilin and αSMA (Fig. 7A), but did not express HSC marker of PROX1 (Fig. 7D). As predicted, HTM/ADSC-derived HSC-like constructs expressed PROX1 at a level similar to that of HTM/HSC constructs (Fig. 7E and 7F). A cross-sectional view of the confocal z-stack showed two distinct layers of cells, with only the HTM cells expressing myocilin (Fig. 7A–C). In addition to lack of myocilin in the HSC or HSC-like layer (Fig. S3 side view and Table S1), these ADSC-derived HSC-like cells expressed HSC markers [57], such as VEGFR2 and VE-cadherin while undifferentiated ADSC did not express these HSC markers (Fig. S4).

We further evaluated the morphology of ADSC-derived HSC-like cells grown on SU8 scaffolds after perfusion (Fig. S5). Like HSC cells, there was minimal cell loss after perfusion in the basal-to-apical direction, which is likely due to the ECM support from the HTM on the opposite side (Fig. S5).

Finally, we examined whether the HTM/ADSC-derived HSC-like construct could respond to an agent that increased flow resistance. Dexamethasone is known to increase flow resistance and IOP, and was used to modulate outflow facility. For analysis of outflow resistance, both HTM/HSC and HTM/ADSC-derived HSC-like constructs were first treated with 100 nM dexamethasone for 3 (Fig. 8A) or 7 days (Fig. 8B), and then placed in the perfusion chamber. The outflow facility in both co-cultures decreased, although the 7-day dexamethasone treatment induced a more significant response in both constructs (Fig. 8B), indicating that HTM/ADSC-derived HSC-like constructs have a similar drug response compared to HTM/HSC constructs. Immunocytochemistry analysis showed that treatment with 100 nM dexamethasone for 7 days induced changes in F-actin organization (compared Fig. 8D with 8C, Fig. 8F with 8E) and increased ECM protein collagen IV and fibronectin

expression (Compared Fig. 8H with 8G, Fig. 8J with 8I) in both HTM/HSC and HTM/ADSC-derived HSC-like constructs. Moreover, ImageJ analysis of DAPI stained cell nucleus revealed significant increase in nuclear size in dexamethasone-treated constructs (Fig. 8K). We also examined the top (HTM cell layer) and bottom (HSC or ADSC-derived HSC-like cell layer) view from confocal images of F-actin expression in HTM/HSC constructs and HTM/ADSC-derived HSC-like constructs. We found more F-actin expression in HTM cells (top layer) than HSC cells or ADSC-derived HSC-like cells (bottom layer) (Fig. S6).

4. Discussion

Schlemm's canal cells play a critical role in regulating aqueous humor removal through formation of intracellular giant vacuoles and pores, making them an attractive target for drug interventions. However, high throughput, *in vitro* preclinical screening of potential drugs requires a large quantity of cells and the scarcity of HSC cells is a bottleneck. To overcome this roadblock in drug discovery, we have attempted to develop an alternative source of HSC-like cells for drug screening purposes. In this study, we investigated the feasibility of differentiating ADSCs into Schlemm's canal-like cells using VEGF-C, shear stress and HTM co-culture on a microfabricated, porous scaffold. Our goal is to differentiate cells that express both vascular (e.g., CD31, VEGFR2) and lymphatic markers (e.g., PROX1, VEGFR3), and exhibit ability to regulate fluidic outflow in response to IOP-modulating agents.

ADSCs are easily obtainable adult stem cells with high expandability and fibroblast-like morphology. Previous studies have shown that co-stimulation of VEGF-A and fluid shear stress could induce formation of cord-like structures, and expression of vascular endothelial markers after 7 days [35–37]. Indeed, similar to previous studies, three-day post-differentiation, treated ADSCs become more elongated and begin to align in the periphery of the culture dish (Fig.1C, E, G). After 11-day treatment, robust cords-like structures, several millimeters in length, could be observed using optical microscopy in cultures treated with both VEGF-A and shear stress (Fig.1H). While treatment with shear stress also induced cord-like formation, it was not nearly as robust as the co-treatment (Fig. 1F). In addition to morphological changes, both shear stress and co-treatment with VEGF-A induced a significant increase in the expression of vascular endothelial markers, CD31 and VEGFR2 (Fig. 2C–D). CD31, also known as platelet endothelial cell adhesion molecule-1, is expressed at high levels at junctions between adjacent endothelial cells [58]. CD31 is expressed in HSC cells of human anterior chambers [59], but not observed in some HSC strains in conventional 2D culture, suggesting likelihood of downregulation during culture [57] while culturing HSC cells on SU8 scaffolds regained CD31 expression [50]. The VEGF-A/VEGFR2 is the most prominent ligand-receptor complex in the VEGF system and is responsible for endothelial cell proliferation, migration, survival, and new vessel formation during angiogenesis [60]. Both CD31 and VEGFR2 are part of a mechanosensory complex that elicits many signaling pathways as a response to fluid shear stress [58]. Therefore, it is no surprise that both growth factor and dynamic stress are necessary to achieve successful endothelial differentiation. Previous findings reported that the combined effect of VEGF-A and shear stress are synergistic in promoting endothelial differentiation

[35]. Our results confirmed that shear stress is critical for inducing endothelial differentiation of ADSCs and combined VEGF-A and shear stress facilitated differentiation to cells that expressed more CD31 and VEGFR2 than VEGF-A-treated ADSCs or vehicle-treated control.

Due to Schlemm's canal's unique identity (lymphatic & vascular), we decided to use a modified protocol for differentiating ADSCs into HSC-like cells. Previous research showed that short-term treatment with VEGF-C induced PROX1 expression but not VEGFR-3 in ADSCs [43]. VEGF-C, a lymphangiogenic growth factor and its receptor, VEGFR-3, are essential for SC development. Delivery of VEGF-C into the adult eye resulted in sprouting, proliferation, and growth of HSC endothelial cells, and was associated with a trend toward a sustained decrease in IOP in adult mice [40]. Recently, VEGFR3 was shown to be a constituent of the mechanosensory complex containing CD31, VE-Cadherin, and VEGFR2. At the onset of shear, VEGFR2 and VEGFR3 are recruited to the mechanosensory complex by the transmembrane domain of VE-Cadherin, followed by phosphorylation of both VEGFR2 and VEGFR3 [58, 61]. These studies suggest that maintenance of Schlemm's canal identity and function may depend on shear stress-induced VEGFR3 expression and downstream signaling.

We determined that treatment with VEGF-C, shear stress, or both, changes the cell morphology from fibroblast-like to elongated (Fig. 3A–J). Gene analysis showed that PROX1 is significantly upregulated in VEGF-C alone treatment, similar to a previous finding [38]. Shear stress also unregulated PROX1, while co-treatment with VEGF-C and shear stress further upregulated PROX1 in comparison to ADSCs. It has been shown that 12-hour-long laminar flow can physically associate KLF4, a key shear stress-responsive transcription factor, with the PROX1 regulatory region in blood endothelial cells, potentially explaining the up-regulation we observed under the shear treatment [62]. Similar to PROX1, VEGFR3 expression is upregulated synergistically by VEGF-C and shear stress co-treatment (Fig. 4A–D), confirming that VEGFR-3 expression is responsive not only to its native ligand, but also shear stress. Western blot analysis (Fig. 4E and G) and immunofluorescence detection (Fig. 5) of the Schlemm's canal-specific markers suggests that VEGF-C alone and co-treatment induced PROX1 expression in ADSC-derived HSC-like cells is comparable to that in primary HSC cells. These results are evidence that combined treatment of VEGF-C and shear stress can induce a Schlemm's canal-like phenotype in ADSCs.

Aside from shear stress, the inner wall endothelium of Schlemm's canal also experiences basal-to-apical flow. This dynamic environment makes it necessary for HSC cells to have strong cellular adhesion to their basement lamina, which include collagen IV, fibronectin, and laminin. These proteins act as structural support, and compensate for mechanical strain, especially around the cell periphery [14, 63]. We reasoned that since the Schlemm's canal's ability to form giant vacuoles and pores depends heavily on basement membrane stiffness, creating an *in vitro* microenvironment with *in vivo*-like substrate stiffness, composition, and porosity is critical not only for maintaining Schlemm's canal phenotype *in vitro*, but also for guiding stem cell differentiation. Previous research by our group demonstrated that bioengineered HTM on microporous SU8 scaffolds exhibit several *in* vivo-like characteristics, such as expression of HTM markers, secretion and remodeling of

surrounding ECM, and most importantly, response to IOP-altering agents [47–50]. Co-culturing ADSCs with this HTM construct could provide the appropriate biological and structural cues to guide ADSC differentiation. To assess whether the co-cultured HTM/ADSC-derived HSC construct possesses the ability to regulate fluid flow, we perfused the construct at various flow rates and monitored the resistance to flow. In addition to morphological similarity, both constructs provided similar resistance to flow, indicating comparable tissue permeability (Fig. 6). Immunocytochemistry confirmed that the HTM/ADSC-derived HSC-like construct not only forms a confluent monolayer that is distinct from the HTM cells (Fig. 7B and E), but expresses levels of PROX1 comparable to those of HSC cells in HTM/HSC constructs (Fig. 7C and F). To determine whether these two constructs behave similarly in terms of flow modulation, they were treated with dexamethasone to induce a decrease in outflow facility. Both constructs showed such a decrease, indicating that ADSC-derived HSC-like cells provide a similar drug response to HSCs when cultured with HTM cells.

Although promising, the potential of using ADSC-derived HSC-like cells in glaucoma drug screening will require further examination. For example, it is important to determine the long-term fate of ADSC-derived HSC-like cells either with or without co-culturing with HTM, as well as their physiological responses to other agents that are known to affect outflow facility. Numerous previous studies have demonstrated the success of using stem cell differentiation techniques for ocular regeneration [64]. The combination of stem cell products with tissue engineering not only offers great potential for tissue and organ repair, but also scalable and modular cell culture systems for cost-efficient stem cell expansion, differentiation, and high-throughput drug screening.

5. Conclusion

In conclusion, we have demonstrated the feasibility of differentiating ADSCs into Schlemm's canal-like cells using VEGF-C, fluidic shear stress, and co-culturing with HTM-scaffold constructs. The differentiated ADSCs expressed characteristic Schlemm's canal markers, PROX1 and VEGFR3. Furthermore, HTM/ADSC-differentiated HSC-like constructs exhibited similar cell morphology, orientation, and coverage on microfabricated porous SU8 scaffolds, as well as outflow facility comparable to HTM/HSC cells, with and without dexamethasone treatment. These findings show that ADSC-derived HSC-like cells have the potential to serve as an alternative cell source to recreate the ocular outflow tract for *in vitro* glaucoma drug screening.

Supplementary Material

Refer to Web version on PubMed Central for supplementary material.

Acknowledgements

References

[1]. Weinreb RN, Leung CKS, Crowston JG, Medeiros FA, Friedman DS, Wiggs JL, Martin KR. Primary open-angle glaucoma. Nat Rev Dis Primers 2016;2:16067.

[2]. Kapetanakis VV, Chan MPY, Foster PJ, Cook DG, Owen CG, Rudnicka AR. Global variations and time trends in the prevalence of primary open angle glaucoma (POAG): a systematic review and meta-analysis. Br J Ophthalmol 2016;100:86–93. [PubMed: 26286821]

[3]. Goel M, Picciani RG, Lee RK, Bhattacharya SK. Aqueous humor dynamics: A review. Open Ophthalmol J 2010;4:52–9. [PubMed: 21293732]

[4]. Weinreb RN, Aung T, Medeiros FA. The pathophysiology and treatment of glaucoma: A Review. JAMA 2014;311:1901–11. [PubMed: 24825645]

[5]. Grant W Experimental aqueous perfusion in enucleated human eyes. Arch Ophthalmol 1963;69:783–801. [PubMed: 13949877]

[6]. Mäepea O, Bill A. The pressures in the episcleral veins, Schlemm's canal and the trabecular meshwork in monkeys: Effects of changes in intraocular pressure. Exp Eye Res 1989;49:645–63. [PubMed: 2806429]

[7]. Ethier CR. The Inner Wall of Schlemm's Canal. Exp Eye Res 2002;74:161–72. [PubMed: 11950226]

[8]. Johnson M 'What controls aqueous humour outflow resistance?'. Exp Eye Res 2006;82:545–57. [PubMed: 16386733]

[9]. Ramos R, Hoying J, Witte M, Stamer DW. Schlemm's canal endothelia, lymphatic, or blood vasculature? J Glaucoma 2007;16:391–405. [PubMed: 17571003]

[10]. Ethier CR, Read AT, Chan D. Biomechanics of Schlemm's canal endothelial cells: Influence on F-actin architecture. Biophys J 2004;87:2828–37. [PubMed: 15454474]

[11]. Fautsch MP, Johnson DH. Aqueous humor outflow: What do we know? Where will it lead us? Invest Ophthalmol Vis Sci 2006;47:4181–7. [PubMed: 17003404]

[12]. Ashpole NE, Overby DR, Ethier CR, Stamer WD. Shear stress-triggered nitric oxide release from Schlemm's canal cells. Invest Ophthalmol Vis Sci 2014;55:8067–76. [PubMed: 25395486]

[13]. Alvarado JA, Betanzos A, Franse-Carman L, Chen J, Gonzalez-Mariscal L. Endothelia of Schlemm's canal and trabecular meshwork: distinct molecular, functional, and anatomic features. Am J Physiol Cell Physiol 2004;286:C621–C34. [PubMed: 14613887]

[14]. VanderWyst SS, Perkumas KM, Read AT, Overby DR, Stamer WD. Structural basement membrane components and corresponding integrins in Schlemm's canal endothelia. Mol Vis 2011;17:199–209. [PubMed: 21264055]

[15]. Braakman ST, Moore JE, Ethier CR, Overby DR. Transport across Schlemm's canal endothelium and the blood-aqueous barrier. Exp Eye Res 2016;146:17–21. [PubMed: 26689753]

[16]. Stamer WD, Braakman ST, Zhou EH, Ethier CR, Fredberg JJ, Overby DR, Johnson M. Biomechanics of Schlemm's canal endothelium and intraocular pressure reduction. Prog Retin Eye Res 2015;44:86–98. [PubMed: 25223880]

[17]. Stack T, Vahabikashi A, Johnson M, Scott E. Modulation of Schlemm's canal endothelial cell stiffness via latrunculin loaded block copolymer micelles. J Biomed Mater Res A 2018;106:1771–9. [PubMed: 29468812]

[18]. Stamer WD, Roberts BC, Howell DN, Epstein DL. Isolation, culture, and characterization of endothelial cells from Schlemm's canal. Invest Ophthalmol Vis Sci 1998;39:1804–12. [PubMed: 9727403]

[19]. Overby DR, Zhou EH, Vargas-Pinto R, Pedrigi RM, Fuchshofer R, Braakman ST, Gupta R, Perkumas KM, Sherwood JM, Vahabikashi A, Dang Q, Kim JH, Ethier CR, Stamer WD, Fredberg JJ, Johnson M. Altered mechanobiology of Schlemm's canal endothelial cells in glaucoma. Proc Natl Acad Sci U S A 2014;111:13876–81.

[20]. Rao PV, Deng P-F, Kumar J, Epstein DL. Modulation of aqueous humor outflow facility by the Rho kinase-specific inhibitor Y-27632. Invest Ophthalmol Vis Sci 2001;42:1029–37. [PubMed: 11274082]

[21]. Inoue T, Tanihara H. Rho-associated kinase inhibitors: A novel glaucoma therapy. Prog Retin Eye Res 2013;37:1–12. [PubMed: 23770081]

[22]. Fraser J, Wulur I, Alfonso Z, Hedrick M. Fat tissue: an underappreciated source of stem cells for biotechnology. Trends Biotechnol 2006;24:150–4. [PubMed: 16488036]

[23]. Housman TS, Lawrence N, Mellen BG, George MN, Filippo JS, Cerveny KA Jr, DeMarco M, Feldman SR, Fleischer AB. The Safety of Liposuction: Results of a National Survey. Dermatol Surg 2002;28:971–8.

[24]. Rodriguez A-M, Elabd C, Delteil F, Astier J, Vernochet C, Saint-Marc P, Guesnet J, Guezennec A, Amri EZ, Dani C, Ailhaud G. Adipocyte differentiation of multipotent cells established from human adipose tissue. Biochem Biophys Res Commun 2004;315:255–63. [PubMed: 14766202]

[25]. Huang H, Song T-J, Li X, Hu L, He Q, Liu M, Lane MD, Tang QQ. BMP signaling pathway is required for commitment of C3H10T1/2 pluripotent stem cells to the adipocyte lineage. Proc Natl Acad Sci U S A 2009;106:12670–5.

[26]. Knippenberg M, Helder MN, Doulabi BZ, Semeins CM, Wuisman PIJM, Klein-Nulend J. Adipose tissue-derived mesenchymal stem cells acquire bone cell-like responsiveness to fluid shear stress on osteogenic stimulation. Tissue Eng 2005;11:1780–8. [PubMed: 16411823]

[27]. Knippenberg M, Helder MN, Zandieh Doulabi B, Wuisman PIJM, Klein-Nulend J. Osteogenesis versus chondrogenesis by BMP-2 and BMP-7 in adipose stem cells. Biochem Biophys Res Commun 2006;342:902–8. [PubMed: 16500625]

[28]. Erickson GR, Gimble JM, Franklin DM, Rice HE, Awad H, Guilak F. Chondrogenic potential of adipose tissue-derived stromal cells in vitro and in vivo. Biochem Biophys Res Commun 2002;290:763–9. [PubMed: 11785965]

[29]. Awad HA, Quinn Wickham M, Leddy HA, Gimble JM, Guilak F. Chondrogenic differentiation of adipose-derived adult stem cells in agarose, alginate, and gelatin scaffolds. Biomaterials 2004;25:3211–22. [PubMed: 14980416]

[30]. Rangappa S, Fen C, Lee EH, Bongso A, Wei ESK. Transformation of adult mesenchymal stem cells isolated from the fatty tissue into cardiomyocytes. Ann Thorac Surg 2003;75:775–9. [PubMed: 12645692]

[31]. Planat-Bénard V, Menard C, André M, Puceat M, Perez A, Garcia-Verdugo J-M, Penicaud L, Casteilla L. Spontaneous cardiomyocyte differentiation from adipose tissue stroma cells. Circ Res 2004;94:223–9. [PubMed: 14656930]

[32]. Rodríguez LV, Alfonso Z, Zhang R, Leung J, Wu B, Ignarro LJ. Clonogenic multipotent stem cells in human adipose tissue differentiate into functional smooth muscle cells. Proc Natl Acad Sci 2006;103:12167–72.

[33]. Safford KM, Hicok KC, Safford SD, Halvorsen Y-DC, Wilkison WO, Gimble JM, Rice HE. Neurogenic differentiation of murine and human adipose-derived stromal cells. Biochem Biophys Res Commun 2002;294:371–9. [PubMed: 12051722]

[34]. Ashjian P, Elbarbary A, Edmonds B, DeUgarte D, Zhu M, Zuk P, Lorenz HP, Benhaim P, Hedrick MH. In vitro differentiation of human processed lipoaspirate cells into early neural progenitors. Plast Reconstr Surg 2003;111:1922–31. [PubMed: 12711954]

[35]. Fischer LJ, McIlhenny S, Tulenko T, Golesorkhi N, Zhang P, Larson R, et al. Endothelial differentiation of adipose-derived stem cells: Effects of endothelial cell growth supplement and shear force. J Surg Res 2009;152:157–66. [PubMed: 19883577]

[36]. dela Paz NG, Walshe TE, Leach LL, Saint-Geniez M, D'Amore PA. Role of shear-stress-induced VEGF expression in endothelial cell survival. J Cell Sci 2012;125:831–43. [PubMed: 22399811]

[37]. Colazzo F, Alrashed F, Saratchandra P, Carubelli I, Chester AH, Yacoub MH, Taylor PM, Somers P. Shear stress and VEGF enhance endothelial differentiation of human adipose-derived stem cells. Growth Factors 2014;32:139–49. [PubMed: 25112491]

[38]. Yang Y, Chen X-h, Li F-g, Chen Y-x, Gu L-q, Zhu J-k, Li P. In vitro induction of human adipose-derived stem cells into lymphatic endothelial-like cells. Cell Reprogram 2015;17:69–76. [PubMed: 25647247]

[39]. Deng J, Dai T, Sun Y, Zhang Q, Jiang Z, Li S, Cao W. Overexpression of Prox1 induces the differentiation of human adipose-derived stem cells into lymphatic endothelial-like cells in vitro. Cell Reprogram 2017;19:54–63. [PubMed: 28055225]

[40]. Aspelund A, Tammela T, Antila S, Nurmi H, Leppänen V-M, Zarkada G, Stanczuk L, Francois M, Makinen T, Saharinen P, Immonen I, Alitalo K. The Schlemm's canal is a VEGF-C/ VEGFR-3-responsive lymphatic-like vessel. J Clin Invest 2014;124:3975–86. [PubMed: 25061878]

[41]. Karpinich NO, Caron KM. Schlemm's canal: more than meets the eye, lymphatics in disguise. J Clin Invest 2014;124:3701–3. [PubMed: 25061871]

[42]. Kizhatil K, Ryan M, Marchant JK, Henrich S, John SWM. Schlemm's canal is a unique vessel with a combination of blood vascular and lymphatic phenotypes that forms by a novel developmental process. PLoS Biol 2014;12:e1001912.

[43]. Yan A, Avraham T, Zampell JC, Haviv YS, Weitman E, Mehrara BJ. Adipose-derived stem cells promote lymphangiogenesis in response to VEGF-C stimulation or TGF-β1 inhibition. Future Oncol 2011;7:1457–73. [PubMed: 22112321]

[44]. Baeyens N, Nicoli S, Coon BG, Ross TD, Van den Dries K, Han J, Lauridsen HM, Mejean CO, Eichmann A, Thomas JL, Humphrey JD, Schwartz MA. Vascular remodeling is governed by a VEGFR3-dependent fluid shear stress set point. eLife 2015;4:e04645.

[45]. Engler AJ, Sen S, Sweeney HL, Discher DE. Matrix elasticity directs stem cell lineage specification. Cell 2006;126:677–89. [PubMed: 16923388]

[46]. Baker BM, Chen CS. Deconstructing the third dimension - how 3D culture microenvironments alter cellular cues. J Cell Sci 2012;125:3015–24. [PubMed: 22797912]

[47]. Torrejon KY, Pu D, Bergkvist M, Danias J, Sharfstein ST, Xie Y. Recreating a human trabecular meshwork outflow system on microfabricated porous structures. Biotechnol Bioeng 2013;110:3205–18. [PubMed: 23775275]

[48]. Torrejon KY, Papke EL, Halman JR, Stolwijk J, Dautriche CN, Bergkvist M, Danias J, Sharfstein ST, Xie Y. Bioengineered glaucomatous 3D human trabecular meshwork as an in vitro disease model. Biotechnol Bioeng 2016;113:1357–68. [PubMed: 26615056]

[49]. Torrejon KY, Papke EL, Halman JR, Bergkvist M, Danias J, Sharfstein ST, Xie Y. TGFβ2-induced outflow alterations in a bioengineered trabecular meshwork are offset by a Rho-associated kinase inhibitor. Sci Rep 2016;6:38319. [PubMed: 27924833]

[50]. Dautriche CN, Szymanski D, Kerr M, Torrejon KY, Bergkvist M, Xie Y, Danias J, Stamer WD, Sharfstein ST. A biomimetic Schlemm's canal inner wall: A model to study outflow physiology, glaucoma pathology and high-throughput drug screening. Biomaterials 2015;65:86–92. [PubMed: 26142779]

[51]. Du Y, Roh DS, Funderburgh ML, Mann MM, Marra KG, Rubin JP, Li X, Funderburgh JL. Adipose-derived stem cells differentiate to keratocytes in vitro. Mol Vis 2010;16:2680–9. [PubMed: 21179234]

[52]. Keller KE, Bhattacharya SK, Borrás T, Brunner TM, Chansangpetch S, Clark AF, Dismuke WM, Du Y, Elliott MH, Ethier CR, Faralli JA, Freddo TF, Fuchshofer R, Giovingo M, Gong H, Gonzalez P, Huang A, Johnstone MA, Kaufman PL, Kelley MJ, Knepper PA, Kopczynski CC, Kuchtey JG, Kuchtey RW, Kuehn MH, Lieberman RL, Lin SC, Liton P, Liu Y, Lütjen-Drecoll E, Mao W, Masis-Solano M, McDonnell F, McDowell CM, Overby DR, Pattabiraman PP, Raghunathan VK, Rao PV, Rhee DJ, Chowdhury UR, Russell P, Samples JR, Schwartz D, Stubbs EB, Tamm ER, Tan JC, Toris CB, Torrejon KY, Vranka JA, Wirtz MK, Yorio T, Zhang J, Zode GS, Fautsch MP, Peters DM, Acott TS, Stamer WD. Consensus recommendations for trabecular meshwork cell isolation, characterization and culture. Exp Eye Res 2018;171:164–73. [PubMed: 29526795]

[53]. Dardik A, Chen L, Frattini J, Asada H, Aziz F, Kudo FA, Sumpio BE. Differential effects of orbital and laminar shear stress on endothelial cells. J Vasc Surg 2005;41:869–80. [PubMed: 15886673]

[54]. Reneman RS, Arts T, Hoeks APG. Wall shear stress - an important determinant of endothelial cell function and structure - in the arterial system in vivo. J Vasc Res 2006;43:251–69. [PubMed: 16491020]

[55]. Yang Y, Chen XH, Li FG, Chen YX, Gu LQ, Zhu JK, Li P. In vitro induction of human adipose-derived stem cells into lymphatic endothelial-like cells. Cell Reprogram 2015;17:69–76. [PubMed: 25647247]

[56]. Torrejon KY. Bioengineering in vitro human trabecular meshwork models for glaucoma therapeutic screening. UMI: University at Albany; 2015.

[57]. Perkumas KM, Stamer WD. Protein markers and differentiation in culture for Schlemm's canal endothelial cells. Exp Eye Res 2012;96:82–7. [PubMed: 22210126]

[58]. Chris G, Ellie T. Endothelial mechanosignaling: Does one sensor fit all? Antioxid Redox Signal 2016;25:373–88. [PubMed: 27027326]

[59]. Heimark RL, Kaochar S, Stamer WD. Human Schlemm's canal cells express the endothelial adherens proteins, VE-cadherin and PECAM-1. Curr Eye Res 2002;25(5):299–308. [PubMed: 12658549]

[60]. Abhinand CS, Raju R, Soumya SJ, Arya PS, Sudhakaran PR. VEGF-A/VEGFR2 signaling network in endothelial cells relevant to angiogenesis. J Cell Commun Signal 2016;10:347–54. [PubMed: 27619687]

[61]. Coon BG, Baeyens N, Han J, Budatha M, Ross TD, Fang JS, Yun S, Thomas JL, Schwartz MA. Intramembrane binding of VE-cadherin to VEGFR2 and VEGFR3 assembles the endothelial mechanosensory complex. J Cell Biol 2015;208:975–86. [PubMed: 25800053]

[62]. Park D-Y, Lee J, Park I, Choi D, Lee S, Song S, Hwang Y, Hong KY, Nakaoka Y, Makinen T, Kim P, Alitalo K, Hong Y K, Koh GY. Lymphatic regulator PROX1 determines Schlemm's canal integrity and identity. J Clin Invest 2014;124:3960–74. [PubMed: 25061877]

[63]. LeBleu VS, MacDonald B, Kalluri R. Structure and function of basement membranes. Exp Biol Med 2007;232:1121–9.

[64]. Stern JH, Tian Y, Funderburgh J, Pellegrini G, Zhang K, Goldberg JL, Ali RR, Young M, Xie Y, Temple S. Regenerating eye tissues to preserve and restore vision. Cell Stem Cell 2018;23:453. [PubMed: 30193132]

Statement of Significance

We successfully generated human Schlemm's canal (HSC) like cells from adipocyte-derived stem cells induced by biochemical and biomechanical cues as well as bioengineered human trabecular meshwork (HTM) on micropatterned, porous SU8 scaffolds. These stem cell-derived HSC-like cells co-cultured with HTM cells on SU8 scaffolds can regulate through-flow, and in particular, are responsive to steroid treatment as expected. These findings show that ADSC- derived HSC-like cells have the potential to recreate the ocular outflow pathway for *in vitro* glaucoma drug screening.

To the best of our knowledge, it is the very first time to demonstrate derivation of Schlemm's canal-like cells from stem cells. It provides an important alternative source to primary Schlemm's canal cells that are very difficult to be isolated and cultured from human donors.
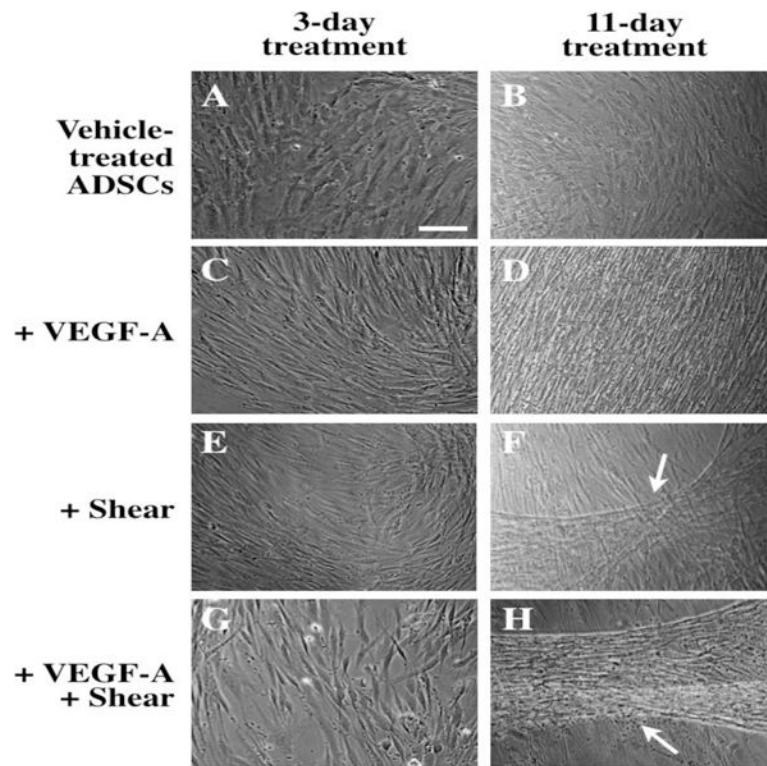
Fig. 1.
Optical images of endothelial differentiation of ADSCs induced by 3-day (A, C, E, G) and 11-day treatment (B, D, F, H) with VEGF-A and shear stress. Vehicle-treated ADSCs (A, B), ADSCs treated with VEGF-A (C, D), shear stress (E, F), or with VEGF-A under shear stress (G, H). White arrows indicate cord-like formation induced by shear stress in the absence (F) or presence of VEGF-A (H). Scale bar = 100 μm.
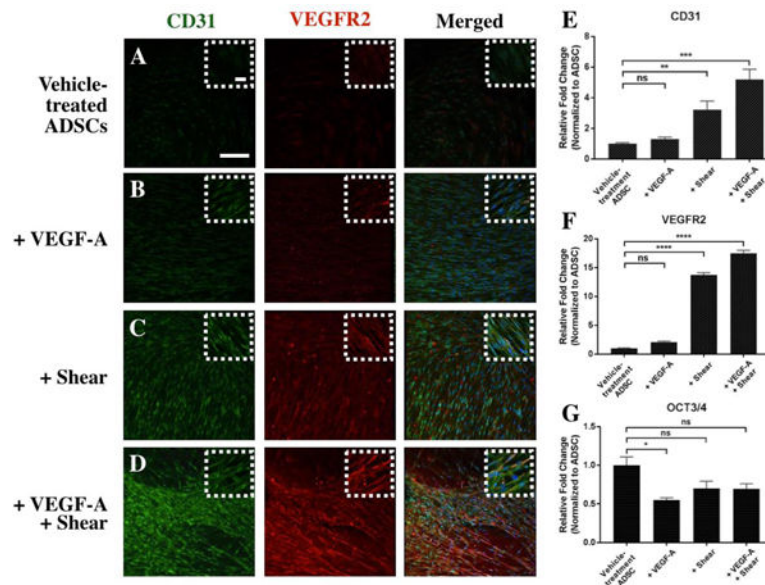
Fig. 2.
Expression of endothelial markers in differentiated ADSCs induced by 11-day treatment with vehicle (A), VEGF-A (B), shear stress (C), or a combination of the two (D). qPCR analysis (E-G) reveals significant increase in expression of endothelial markers (CD31 and VEGFR2) and decreased expression of stem cell marker OCT3/4 as a result of these stimulation. Scale bar = 100 μm. *$p < 0.01$, **$p < 0.001$, ***$p < 0.0005$, ****$p < 0.0001$, ns: not significant.
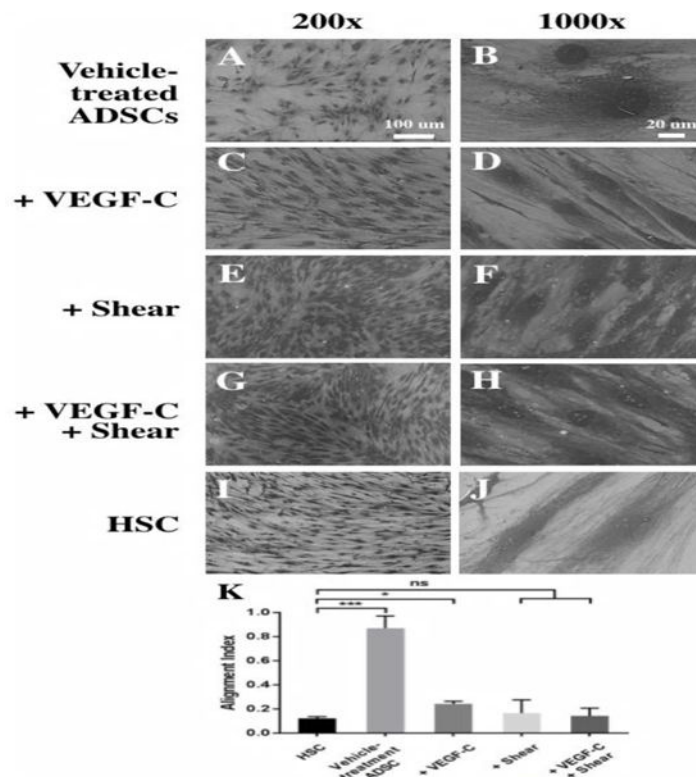
Fig. 3.
Differentiation of ADSCs into Schlemm's canal-like cells induced by VEGF-C and shear stress for 11 days. SEM images of ADSCs at 200× (A, C, E, G, I) and 1000× (B, D, F, H, J) showed dramatic changes in cell morphology and orientation. Vehicle-treated ADSCs (A, B), ADSCs treated with VEGF- C (C, D), shear stress (E, F), or with VEGF-C under shear stress (G, H), and primary HSC cells as the positive control (I, J). Scale bars: (A, C, E, G, I) 100 μm, (B, D, F, H, J) 20 μm. (K) Quantitative analysis of the degree of cell orientation based on the alignment index. A high alignment index represents high randomness of cell orientation. HSCs and differentiated ADSCs are much more oriented than vehicle-treated ADSCs. $*p < 0.01$, $***p < 0.0005$, ns: not significant.
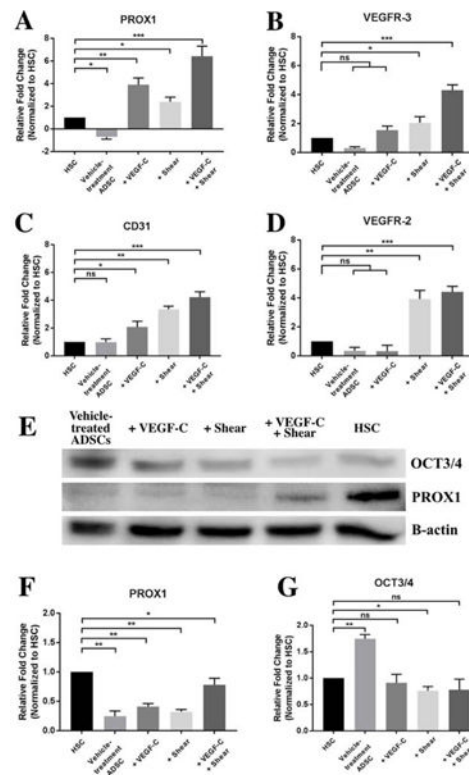
Fig. 4.
Expression of characteristic HSC markers in ADSCs after 11-day treatment with VEGF-C and shear stress. qPCR analysis of gene expression of HSC markers of PROX1 (A), VEGFR3 (B), CD31 (C), and VEGFR2 (D). Representative immunoblot (E) and densitometric analysis of HSC marker PROX1 (F) and stem cell marker OCT3/4 (G). *p < 0.01, **p < 0.001, ***p < 0.0005.
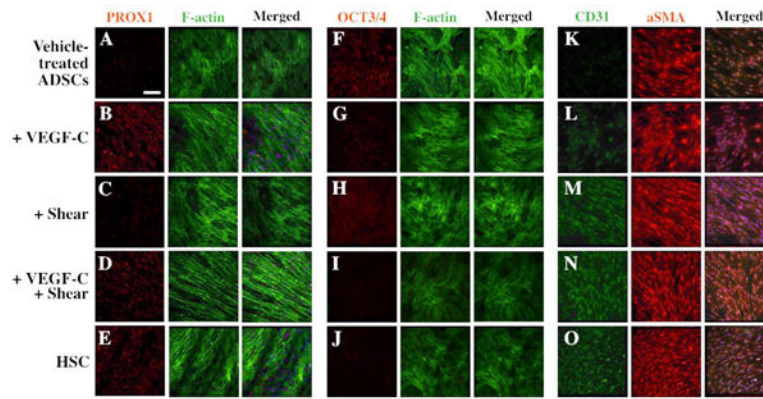
Fig. 5.
Confocal images of HSC marker expression in vehicle-treated ADSCs (A, F, K), ADSCs treated with VEGF-C (B, G, L), shear stress (C, H, M) or VEGF-C and shear stress (D, I, N), and HSC cells (E, J, O). Cells were costained with phalloidin to label F-actin (A-J) or with αSMA (K-O). Scale bar = 100 μm.
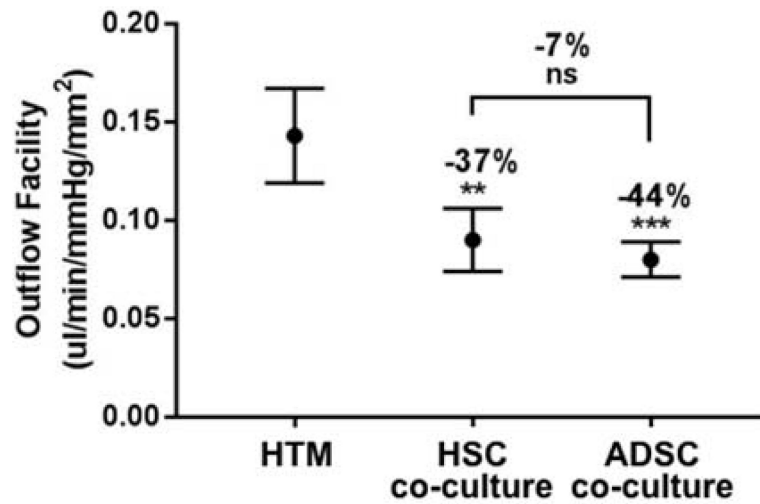
Fig. 6.
Perfusion studies of the outflow facility of 3D HTM, HTM/HSC and HTM/ADSC-derived HSC- like constructs mimic the trabecular outflow tract. Outflow facility is similarly reduced in both HTM/HSC and HTM/ADSC-derived HSC-like constructs compared with that of HTM alone constructs. **p < 0.001, ***p < 0.0005, ns: not significant.
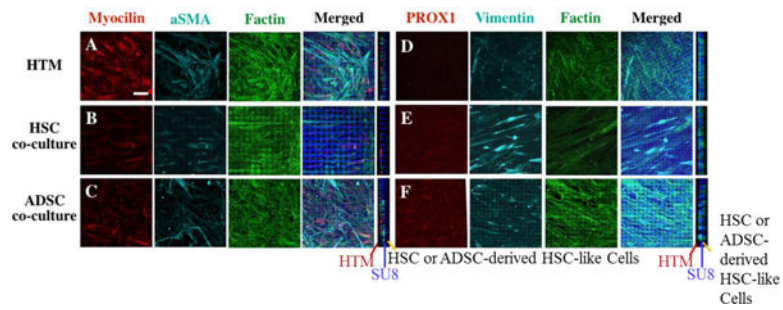
Fig. 7.
Confocal images of expression of HTM and HSC markers in HTM, HTM/HSC and HTM/ ADSC- derived HSC-like constructs on SU8 scaffolds after perfusion. Expression of HTM markers myocilin and αSMA (A, B, C) and HSC marker PROX1 (D, E, F). Constructs were co-stained with F-actin (A, B, C, D, E, F) and vimentin (D, E, F) as well as DAPI to reveal nuclei, along with crossectional view in the left panel (middle blue line showed the SU8 scaffold, HTM cell on the left side of the scaffold and HSC or ADSC-derived HSC cells on the right side of the scaffold). Scale bar = 50 μm.
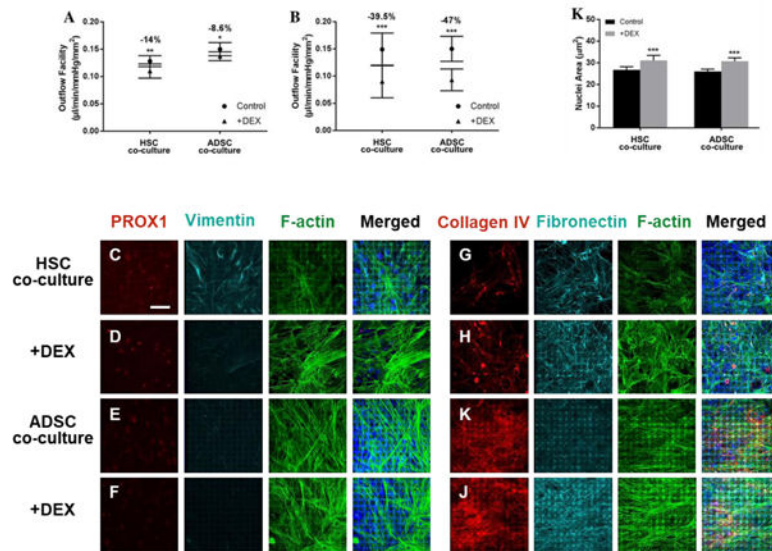
Fig. 8.
Dexamethasone-induced responses to outflow in HTM/HSC and HTM/ADSC-derived HSC-like constructs after 3 (A) and 7 days (B) of treatment. Confocal images of expression of HSC marker and ECM protein in the HSC or ADSC-derived HSC-like cell layer of the co-cultured constructs with or without 7-day dexamethasone treatment. Expression of HSC marker PROX1 (C, D, E, F) and ECM protein of Collagen IV and fibronectin (G, H, I, J). Constructs were co-stained with vimentin (C, D, E, F) and F-actin (C, D, E, F, G, H, I, J) as well as DAPI to label nuclei. Scale bar = 50 μm. (K) Quantification of nuclear size after dexamethasone treatment compared to control. *p < 0.01, **p < 0.001, ***p < 0.0005.

Table 1.

The sequence of the primer set used in this study

Name	Forward	Reverse
PROX1	5'-TAC GCA CGT CAA GCC ATC AA-3'	5'-CAG GAA TCT CTC TGG AAC CTC A-3'
VEGFR3	5'-GCA CCG AGG TCA TTG TGC-3'	5'-CCT CCA GTC ACG GCA C-3'
CD31	5'-ATT GCT CTG GTC ACT TCT CC-3'	5'-CAG GCC CAT TGT TCC C-3'
VEGFR2	5'-GGA AGC TCC TGA AGA TCT GT-3'	5'-GAG GAT ATT TCG TGC CGC-3'
OCT3/4	5'-TGA GTA GTC CCT TCG CAA GC-3'	5'-TTA GCC AGG TCC GAG GAT CA-3'
GAPDH	5'GAT TCC ACC CAT GGC AAA TTC-3'	5'-GTC ATG CCT TCC ACG ATA C-3'